Wavefront Control Testbed (WCT) experiment results

Laura A. Burns [a*], Scott A. Basinger [b], Scott D. Campion [c], Jessica A. Faust [b], Lee D. Feinberg [d], Joseph J. Green [b], William L. Hayden [d], Andrew E. Lowman [b], Catherine M. Ohara [b], Peter P. Petrone III [e], David C. Redding [b], Fang Shi [b], David Van Buren [b], Barbara Zukowski [c]

[a] Science Systems and Applications Inc., 10210 Greenbelt Rd Suite 600, Lanham MD;
[b] Jet Propulsion Laboratory, California Institute of Technology,
4800 Oak Grove Drive, Pasadena, CA 91109;
[c] Swales Aerospace, 5050 Powder Mill Rd., Beltsville, MD 20705;
[d] NASA Goddard Space Flight Center, Greenbelt, MD 20771;
[e] Sigma Space, 4801 Forbes Blvd., Lanham, MD 20706;

ABSTRACT

The Wavefront Control Testbed (WCT) was created to develop and test wavefront sensing and control algorithms and software for the segmented James Webb Space Telescope (JWST). Last year, we changed the system configuration from three sparse aperture segments to a filled aperture with three pie shaped segments. With this upgrade we have performed experiments on fine phasing with line-of-sight and segment-to-segment jitter, dispersed fringe visibility and grism angle;. high dynamic range tilt sensing; coarse phasing with large aberrations, and sampled sub-aperture testing. This paper reviews the results of these experiments.

Keywords: James Webb Space Telescope, JWST, Next Generation Space Telescope, NGST, Wavefront Control Testbed, WCT, DCATT, active optics, segmented optics, wavefront sensing, wavefront control, phase retrieval

1. INTRODUCTION

Currently under development, James Webb Space Telescope is a large, segmented aperture telescope. JWST's primary mirror size and segmentation has provided many challenges for aligning and testing the telescope. Over the past seven years, the Wavefront Control Testbed (WCT) has been working to unravel some of those challenges.

The WCT is an optical system residing at NASA's Goddard Space Flight Center in Greenbelt, MD. Over the past seven years, many papers have been written regarding WCT hardware[ref], experimentation[ref], algorithms[ref], and software[ref]. This paper attempts to summarize results from WCT since the last conference.

First, the background of WCT is presented discussing its various hardware iterations. Secondly, we discuss improvements made to the testbed since last presented. Finally we discuss some interesting experiment results.

2. BACKGROUND

Planning for what would eventually become the Wavefront Control Testbed (WCT) began in 1996. At the time, JWST, called the Next Generation Space Telescope, was still in the planning and technology development phase. This testbed was designed to provide a hardware platform in order to test the wavefront sensing and control algorithms in a real world situation. Initially the optical system was called the Developmental Cryogenic Active Telescope Testbed (DCATT).

The plan for DCATT was a double pass system with a segmented one meter primary mirror. [ref] Due to hardware problems with the actuators and mirror manufacturing, this plan was abandoned. While the primary mirror assembly was scrapped, the base infrastructure was still an important resource fro the project. For a brief time, the testbed was tied to a flight proposal called NEXUS, but eventually, it became simply WCT.

* Laura.A.Burns@gsfc.nasa.gov; phone 301-286-9830; fax 301-286-3133; NASA Goddard Space Flight Center, Mail Stop 443, Greenbelt, MD, 20771-001; JWST's WCT Web Site: http://www.jwst.nasa.gov/Hardware/text/WCT.html

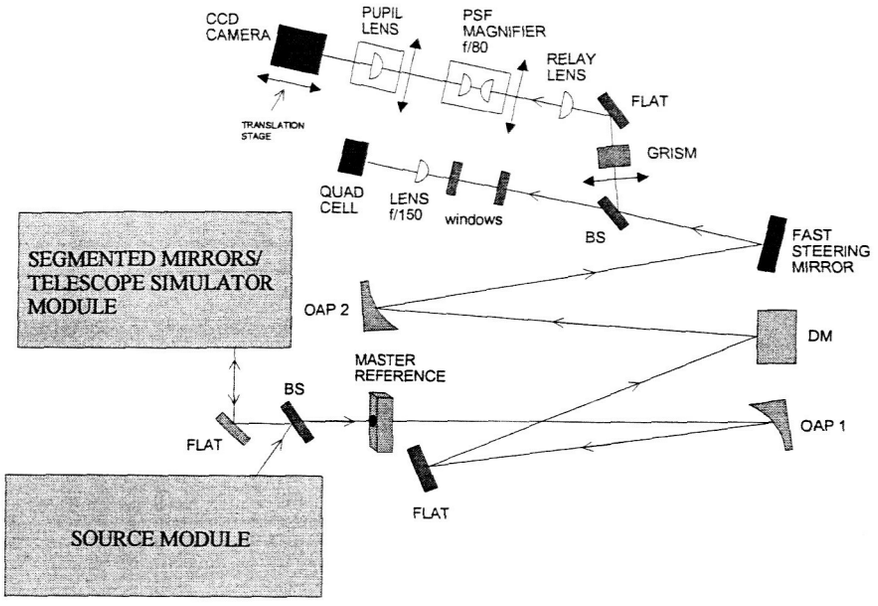

Figure 1: Wavefront Control Testbed Optical Diagram

The optical diagram of WCT is shown in Figure 1. The system consists of three modules, the source module, the telescope simulator module (TSM), and the aft optics. Figure 1 shows the aft optics in some detail. Figure 4 below shows the telescope simulator module in more detail. Of note is the xenon lamp in the source module providing broadband light and the 349 actuator Xianetics deformable mirror and fast steering mirror, both in the aft optics. More information on the hardware configuration of the systems can be found in references [x] and [y].

Since the original primary mirror assembly was cancelled, WCT progressed through a series of gradual upgrades to the TSM, shown in Table 1. Each successive configuration mode added a new aspect to the testbed and therefore a new challenge for the algorithms. These modes are mutually exclusive. Due to the upgrade to WCT-3, WCT-2 is no longer available. Section 3 will discuss this transition in more detail.

Table 1: Wavefront Control Testbed Configuration Modes

Configuration Mode	**Hardware Involved**
WCT – ½	Discrete phase plates
WCT – 1	TSM deformable mirror, monolithic controllable surface
WCT – 2	Three round, spherical mirror segments creating a sparse aperture, segments are controllable via actuators providing three degrees of freedom
WCT – 3	Three pie shaped, spherical mirror segments creating a X% filled aperture, segments are controllable via actuators providing three degrees of freedom

While the WCT hardware is physically located at NASAGSFC, we have worked with many people spread across the country over the course of the project. Primary team contingents have been at GSFC and JPL. This team organization has, at times, created challenges of its own. Our custom software was designed with remote capability in mind to accommodate the team dynamic. Through the various challenges and phases, the team continued to perform well together regardless of physical location.

3. HARDWARE UPDATES

As part of the series of successive improvements, we have upgraded our system from WCT-2 to WCT-3. This gave us an aperture, while is not close to that of JWST, is significantly more traceable. Figure 2 is a photograph of the WCT-2 mirrors prior to the upgrade. The photograph in Figure 3 shows the system after the WCT-3 upgrade. Figure 4 is an optical diagram of the WCT telescope simulator module (TSM) to provide context. With WCT-3 in place, we can still access WCT-1 and WCT-½ via a translation stage or filter wheel respectively.

Figure 2: WCT-2 Hardware

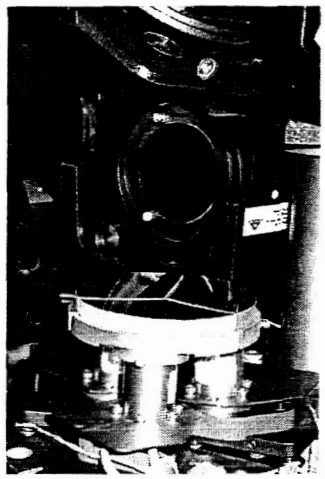

Figure 3: WCT-3 Hardware

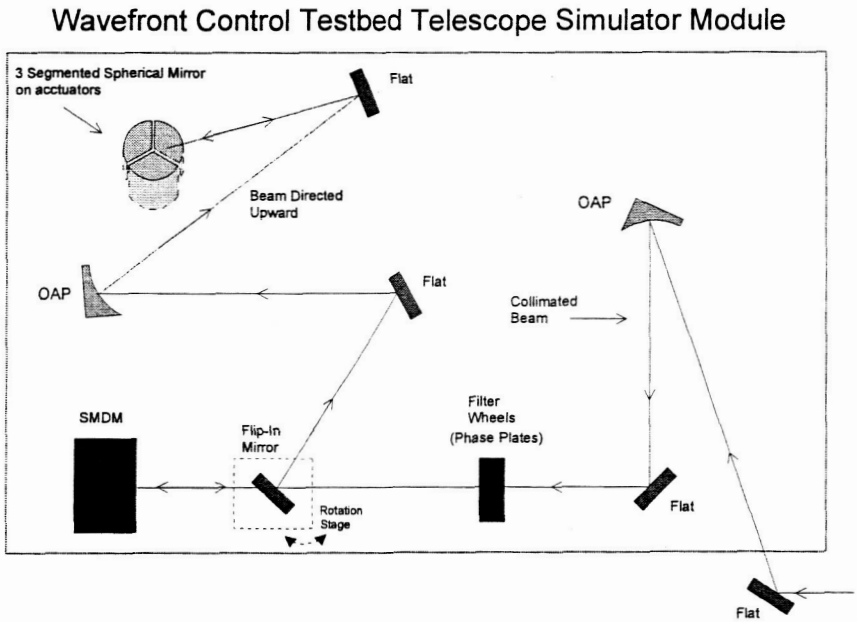

Figure 4: Wavefront Control Testbed Simulator Module

The potential for upgrades was taken into account in the original WCT-2 design. The mirror segments were designed to be easily removed from the actuators and others installed. While the removal of the WCT-2 mirrors went smoothly, the installation of the WCT-3 mirrors did not. The tolerance on the mirror mount was too tight. Time pressures prohibited re-fabrication and the segments had to be forced onto the actuator interface. As a result, we experienced significant mirror deformations.

During an attempt to re-mount one segment, we encountered a catastrophic failure of the actuator assembly. Fortunately, this was an understood risk prior to the re-mounting process. A replacement actuator assembly was available. The segment was quickly mounted on the new actuator assembly and reinstalled. It was necessary to re-calibrate the segment motion as well. The efforts used to address this problem via experimentation are described in more detail in Section 4.4.

4. EXPERIMENT RESULTS

4.1 Fine Phasing Jitter Experiments

One of the last set of experiments run on WCT was a series of jitter experiments. The goal of these experiments was to understand the behavior of the basic algorithm process in the presence of jitter.

We conducted experiments with line-of-sight and segment-to-segment jitter. The line-of-sight jitter was induced using a fast steering mirror located in the aft optics. The segment-to-segment jitter was induced using a built-in capability of the PZT actuators. In both cases, it was possible to define the type of movement.

Overall we ran fifteen different sets of jitter data, three used line-of-sight jitter and twelve used segment to segment jitter. When taking the imagery, the exposure times were calculated such that several cycles of jitter occurred during each frame. Multiple frames were used in the creation of one pre-processed image used for phase retrieval. We induced sine wave and random motion. For segment-to-segment motion many configurations were possible. Data was taken with one segment jittering or all segments jittering. The movement could be in tip, tilt, or piston. For sine wave motion, data was taken with a radial jittering motion.

Our focus diversity mechanism for WCT is to translate our CCD camera by a given number of millimeters. To add another dimension to the experiments, we always took two sets of defocus images. The large defocus sets were translated by +/- 25 mm and +/- 12.5 mm. This equates to +/- [X] waves and +/- [X] waves of defocus. The small defocus sets were translated by +/- 5 mm and +/- 3 mm. This equates to +/- [X] waves and +/- [X] waves of defocus.

The jitter levels induced are reported in terms of number of pixels moved in the in focus image. The jitter gain level was calculated by observing sine wave jitter in the in focus image. This information was then used to scale the jitter to the level desired. No jittered images are presented here since the jitter levels used are difficult to see with the naked eye.

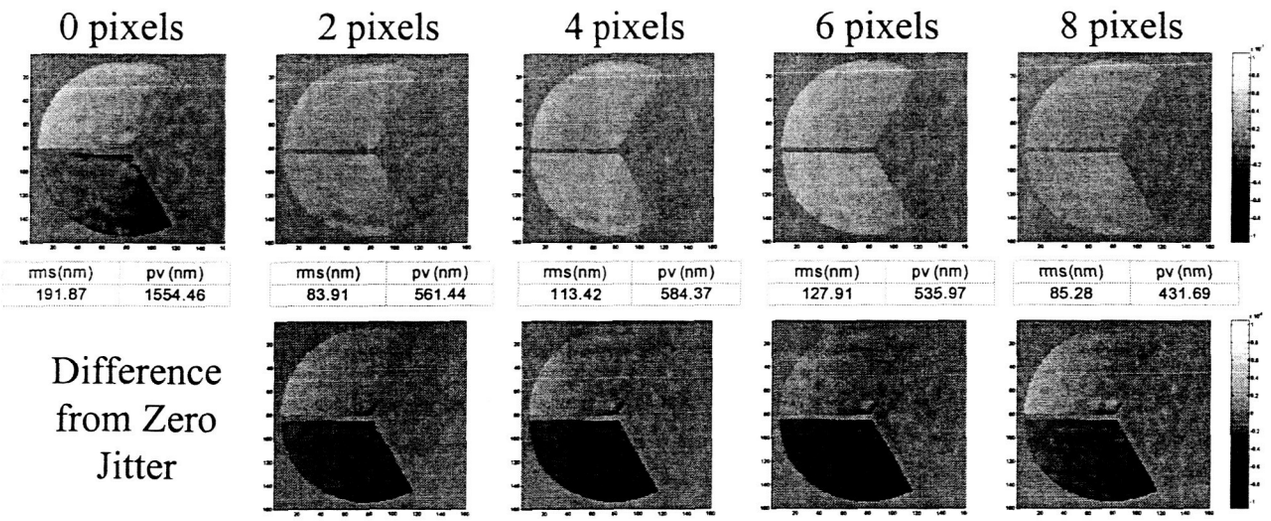

Figure 5: Phase Estimate Calculated Using Large Defocus Images

All data sets were processed using the standard MGS algorithms. The phase retrieval process included using a non-jittered pupil image. When calculating the tip, tilt, and piston levels in the wavefront estimate, segment one was defined as the reference segment. This segment was chosen based off of our understanding of the segment behavior patterns. The plane of this segment was subtracted from the other two. The resulting tip, tilt and piston was calculated from there.

For simplicity, we are presenting the detailed results of only one of these experiments. In this experiment, we induced random, segment-to-segment jitter. The system was first put in its optimal, "flattened" state. We moved segment three in piston by 100 nm. The system was left in this configuration throughout the entire experiment.

Figure 5and Figure 6 show the calculated wavefront estimates for the various levels of jitter. All of these wavefront estimates and difference image are displayed on the same color scale. The aft optics deformable mirror causes the high frequency waffle pattern in the images. In both cases, the jitter washes out this high frequency aberration. In the estimates created by the small defocused image, phase wrapping[ref] artifacts are induced in the 8 pixel jitter case. This is evidenced by the abrupt changes in coloration within the estimate.

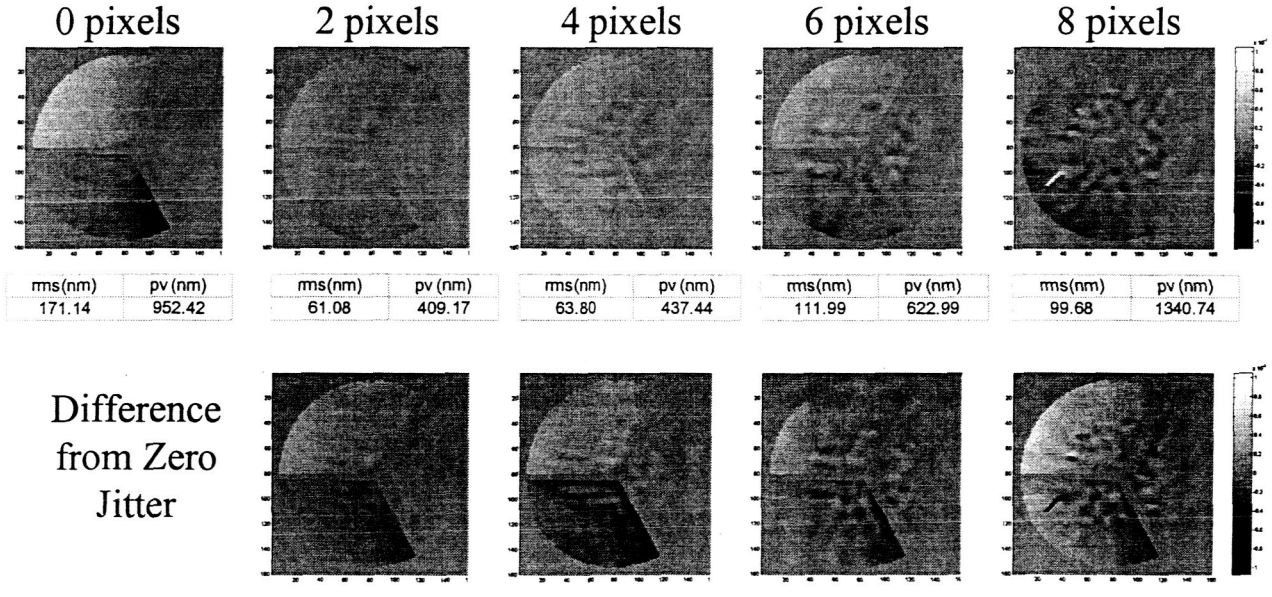

Figure 6: Phase Estimate Calculated Using Small Defocus Images

Figure 7 to Figure 12 show the detected aberration level versus the number of pixels of jitter. This case, as do the other experiments, shows that the algorithms do not identify tip, tilt, and piston, in the presence of jitter with any reliability. This is true regardless of the level of defocus induced.

There are several things that affect this result. Firstly, most of the test cases were of our nominally "flat" system. The level of aberration in the base system was usually less than 70 nanometers rms wavefront error. The system detection repeatability level is [x]. For a better test of the system detection capability, we should have induced error at a variety of levels in the system. While we could control the system to the sub-pixel level, we did not adequately examine the jitter range between zero and one pixel of jitter. The levels we used were extreme based on the system configuration.

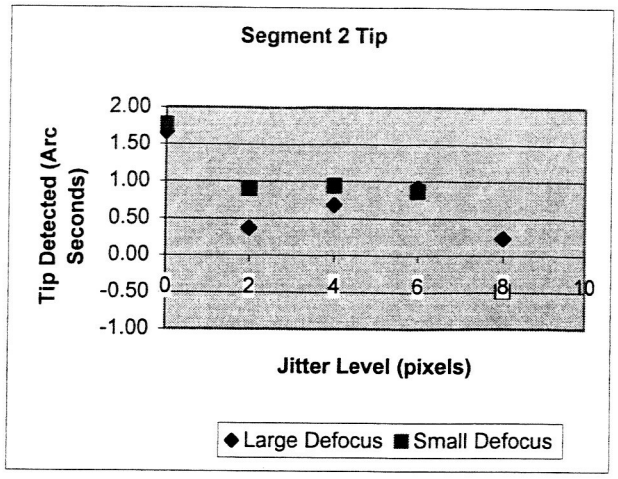

Figure 7: Segment 2 Tip

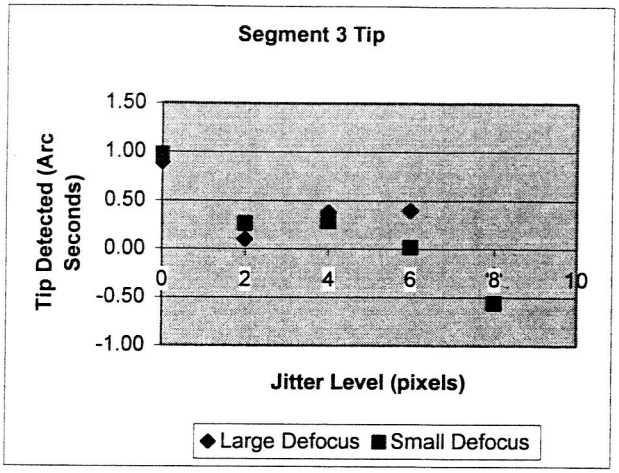

Figure 10: Segment 3 Tip

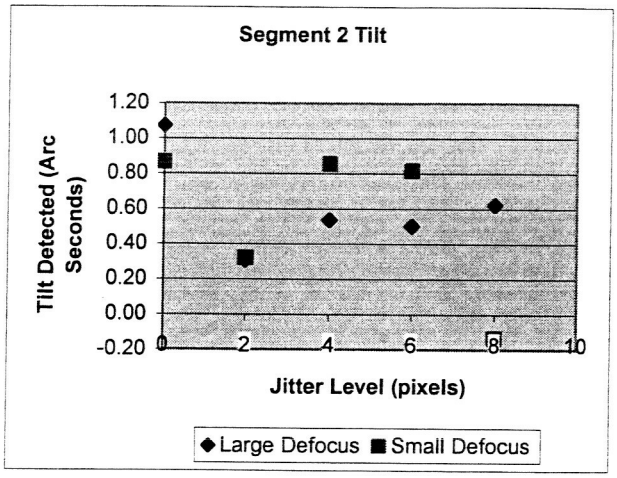

Figure 8: Segment 2 Tilt

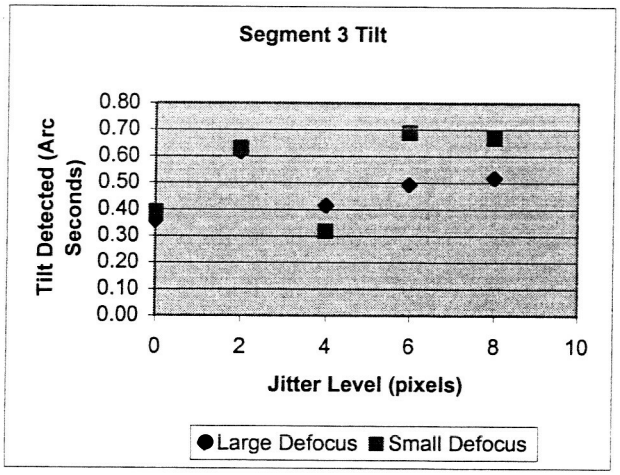

Figure 11: Segment 3 Tilt

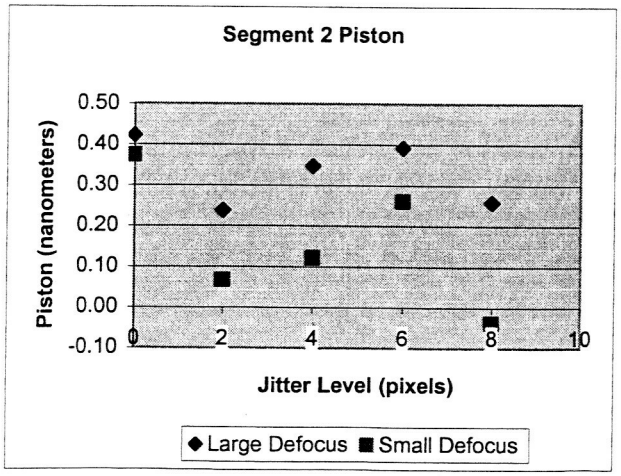

Figure 9: Segment 2 Piston

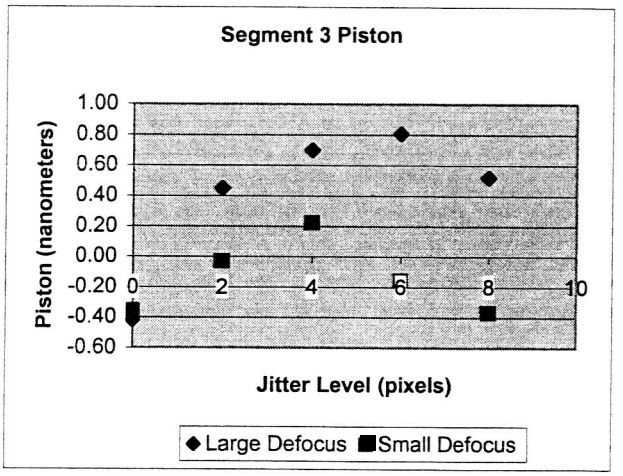

Figure 12: Segment 3 Piston

4.2 Grism rotation

The coarse phasing mechanism used on WCT is dispersed fringe sensing. The process used has been described in detain in several papers by Shi. [Ref] Throughout the lifetime of WCT, we have been studying various ways to optimize the dispersed fringe sensor (DFS) fringe visibility. Example WCT-3 fringes are shown in Figure 13.

DFS fringe visibility depends strongly on the relative orientation of grism dispersion direction and the segment mirror baseline. Visibility also depends on pixel sampling, the mirror segments' aperture shape, the mirror area difference, the aperture sparseness, and any aberrations present. For any given segment pair, maximum visibility occurs when the dispersion is perpendicular to the segment baseline. As the grism is rotated from the perpendicular, the visibility drops to zero. This decline in fringe modulation happens faster with a sparse aperture.

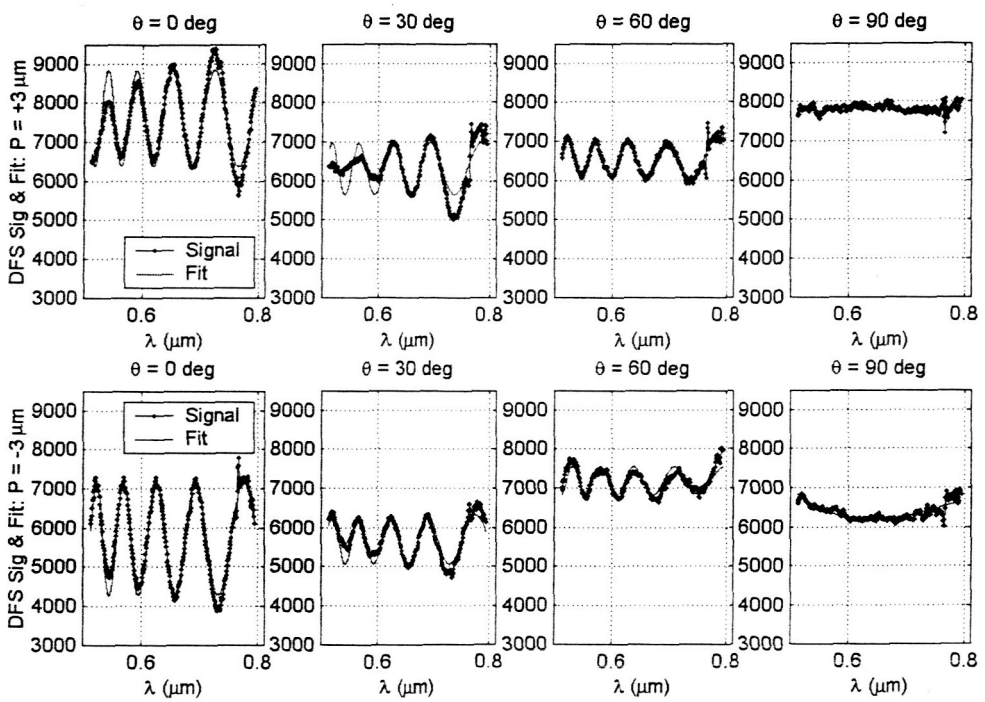

Figure 13: WCT-3 Sample DFS fringes and DFS Fits

The grism in the WCT system is on a 360° rotation stage. This allowed us to measure the fringe visibility over the entire range. This experiment began with WCT-2 and the initial results were presented in [ref]. Repeating the experiment with WCT-3 we are able to examine the effect of the aperture shape on the visibility.

Shown if Figure 14, the WCT-3 DFS fringe visibility gradually declines over the angular range. It does not approach zero until the grism dispersion is virtually parallel to the segment baseline. The detection error remains small for all but the extreme cases. Figure 16 shows the WCT-2 visibility. With the sparse aperture, DFS visibility progresses to zero after only 25° in either direction.

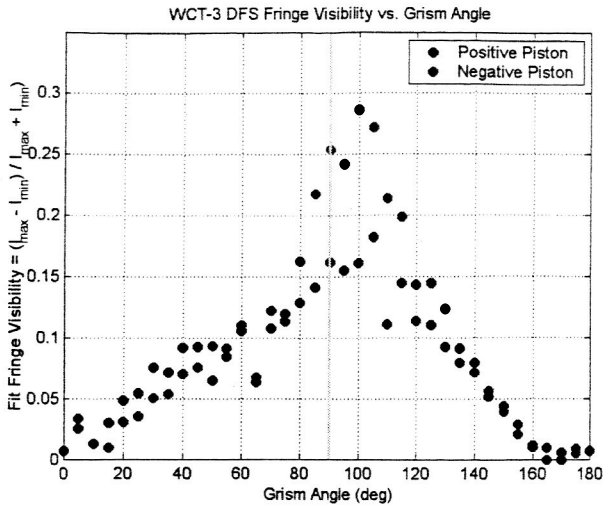

Figure 14: WCT-3 DFS Fringe Visibility versus Grism Angle

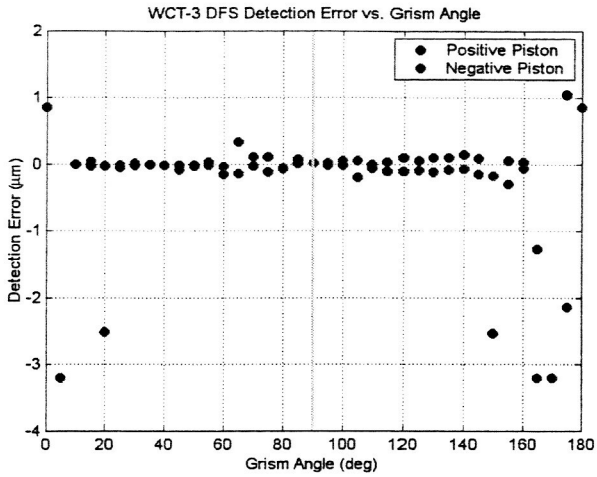

Figure 15: DFS Detection Error versus Grism Angle

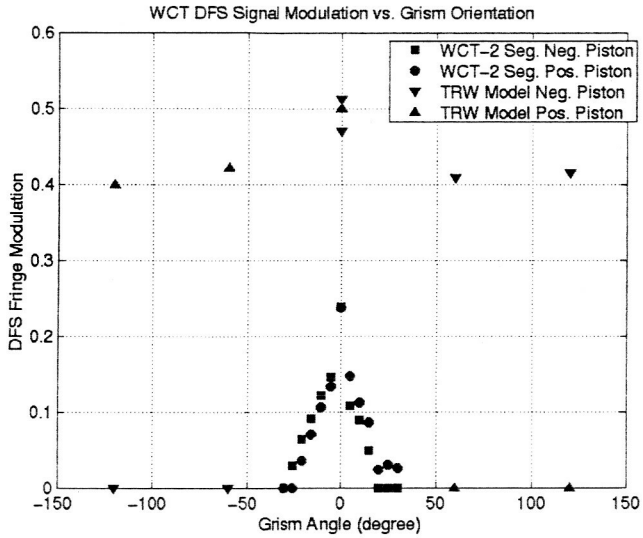

Figure 16: WCT-2 and 36 Kex Model Result

4.3 Large tilt sensing

This experiment was designed to determine if focus-diverse phase retreieval ccoudl adequately detect high dynamic range tilt errors.

Beginning with a well phased system, we then sent incremental tilt commands to the segment PZT actuators. At each step, we collected defocus imagery for phsase retrieval processing. Shown in Figure 17, we collected 4 defocused imagese and an in focus image. The infocus image is only used for comaproison. It was not used for phase retreival processing. The expamle images contain [x] arcseconds of tilt. These pictres were taken using a broadband source. Additional data was taken using a narrow band (20 micron bandwidth) source.

The MGS unwrapping procedure uses a combination of raster unwrapping and "outer-outer" loop Zernike fitting across individual segments. Figure 18, Figure 19, and Figure 20 show the detectecd tilt versus commanded tilt for segmets 1, 2, and 3 respectively. Table 2 summarizes the residual detection scatter.

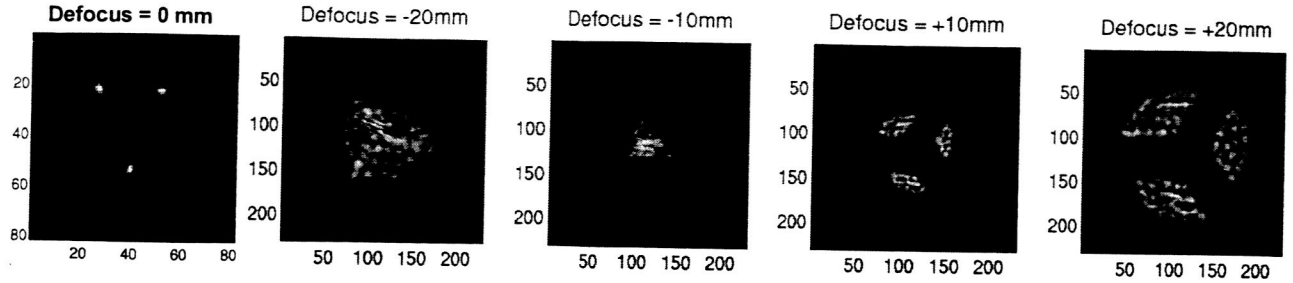

Figure 17: Sample infocus psf and 4 defocused images used in large tilt sensing phase retrieval

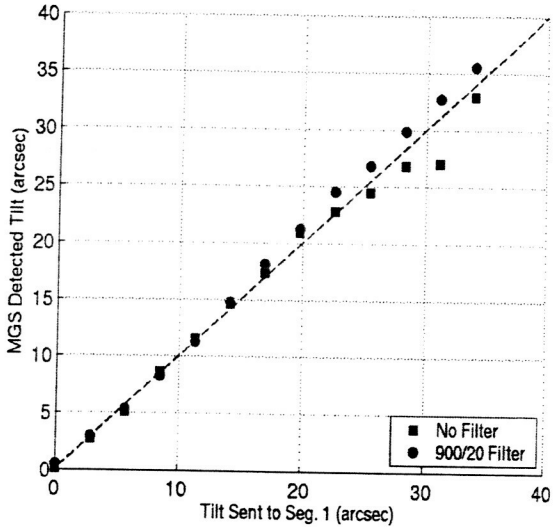

Figure 18: Detected Tilt versus Commanded Tilt for Segment 1

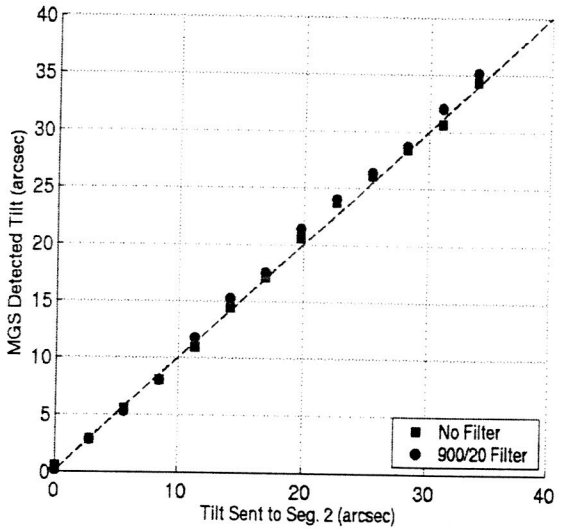

Figure 19: Detected Tilt versus Commanded Tilt for Segment 2

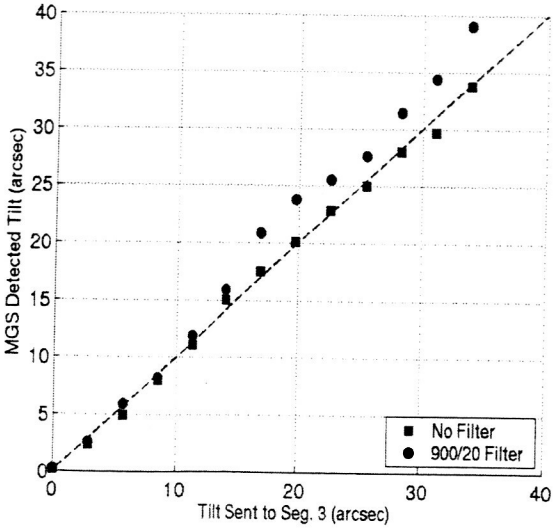

Figure 20: Detected Tilt versus Commanded Tilt for Segment 3

Table 2: Residual Scatter

	Segment 1	Segment 2	Segment 3
Broadband Source	1.1 arcsec	0.5 arcsec	0.6 arcsec
Narrowband Source	0.4 arcsec	0.4 arcsec	0.9 arcsec

Through this experiment we were able to show that the measure large segment-tilt errors reasonably well. Possible applications of this approach include improving the overall phasing effort by correcting residual tilts after coarse image stacking or refining tilt errors during DFS coarse phasing.

4.4 Sensing with segment aberrations

After the initial instillation of WCT-3, we were left with wavefront errors much higher than expected. These errors were interfering with the initial phasing of WCT-3. In order to determine the level of error, we moved all but one segment out of the immediate field of view. We then took focus diverse phase retrieval data for each segment individually. After processing these data, we were able to reconstruct the overall phase map. The aft-optics deformable mirror could then be used to compensate for the error. Figure 21 shows the reconstructed phase map with the piston, tip, tilt, and spherical Zernike terms removed. The lighter colored patch in the center of each segment appears to be the primary mounting point of each segment.

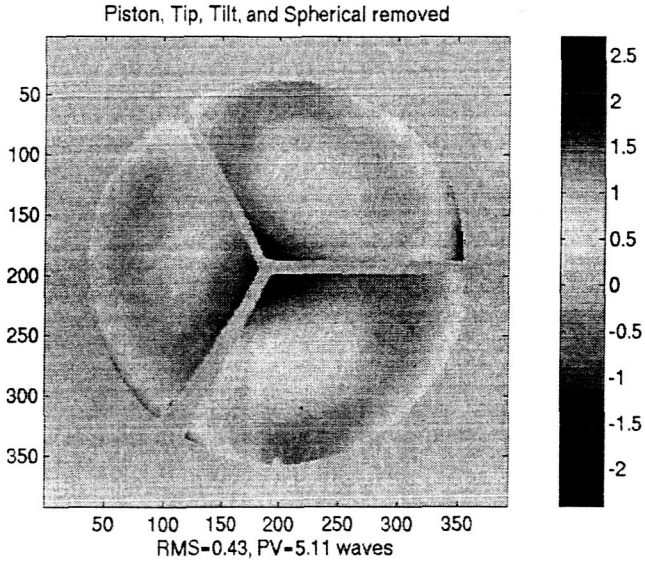

Figure 21: Early WCT-3 Image showing mounting induced aberrations

4.5 Sampled Sub Aperture

One feature of the WCT-3 configuration is its mapping to the sampled sub-aperture testing configuration to be used on JWST during ground testing. The three pie shaped segments are analogous to a sub-aperture of there hexagonal segments. Using this aspect of WCT-3 and the aft-optics deformable mirror, we simulated radius of curvature error on a hexagonal segment. More information on these results is available in [ref]

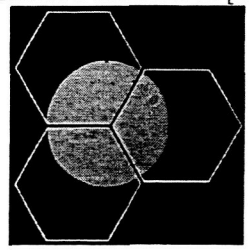

Figure 22: WCT-3 mapping to a sub aperture of three hexagonal segments

5. CONCLUSION

Over the past seven years WCT has produced important results that have furthered the JWST project and the study of wavefront sensing and control. While, further experimentation on WCT could produce valuable results, the resources and study need to progress to more complex optical systems.

ACKNOWLEDGEMENTS

The authors would to thank everyone who worked on WCT in its various incarnations over the years. This includes: T. Antczak, C. Aviado, T. Beck, P. Bely, G. Blackhall, R. Boucarut, C. Bowers, J. Britt, M. Bussman, R. Burg, Q. Chau, A. Chu, D. Cohen, D. Coulter, P. Davila, B. Dean, J. Deering, P. Dogoda, W. Eichhorn, M. Fitzmaurice, R. Fedorchak, P. Geithner, K. Ha, J. Hagopian, T. Hanyok, H. Hall, K. Harvel, S. Irish, D. Jacobsen, R. Keski-Kuha, C. LeBoef, J. Lecha, D. Lindler, K. Liu, X. Liu, J. Mather, P. Maymon, R. Morris, A. Morell, G. Mosier, T. Norton, J. Offenberg, L. Pacini, B. Palfy, B. Perkins, C. Perrygo, D. Robinson, P. Sabelhaus, B. Saif, J. Schott, B. Seery, R. Sengupta, A. Sivaramakrishnan, D. Skelton, S. Stoner, D. Tonnu, L. Wheeler, M. Wilson, L. Worrel, E. Young, and all those others who worked behind the scenes to make WCT a success

REFERENCES

1. L. Burns, S. Basinger, et al, "Wavefront Control Testbed integrated software system," Proc. SPIE 4850-58, Waikoloa, Hawaii, 2002.
2. S. Basinger, L. Burns, et al, "Wavefront sensing and control software for a segmented space telescope," Proc. SPIE 4850-56, Waikoloa, Hawaii, 2002.
3. P. Petrone, B. Zukowski, et al, "Optical design and performance of the NGST wavefront control testbed," Proc. SPIE 4850-55 Waikoloa, Hawaii, 2002.
4. F. Shi, A. Lowman, et al, "Segmented mirror coarse phasing with a dispersed fringe sensor: experiments on NGST's wavefront control testbed," Proc. SPIE 4850-51, Waikoloa, Hawaii, 2002.
5. F. Shi, C. Ohara, et al, "Segmented mirror coarse phasing with white light interferometry: modeling and experimenting on NGST's wavefront control testbed," Proc. SPIE 4850-59, Waikoloa, Hawaii, 2002.
6. D. Cohen, D. Redding, "NGST high dynamic range unwrapped phase estimation," Proc. SPIE 4850-52, Waikoloa, Hawaii, 2002.
7. C. Ohara, D. Redding, et al, "PSF monitoring and in-focus wavefront control for NGST," Proc. SPIE 4850-64, Waikoloa, Hawaii, 2002.
8. S. Basinger, D. Redding, et al, "Performance of wavefront sensing and control algorithms on a segmented telescope testbed," Proc. SPIE 4013-52, Munich, Germany, 2000.
9. C. Bowers, P. Davila, et al, "Initial test results from the Next Generation Space Telescope (NGST) Wavefront sensing and Control Testbed (WCT)," Proc. SPIE 4013-116, Munich, Germany, 2000.
10. A. Lowman, F. Shi, et al, "Telescope simulator for the Nexus wavefront control testbed," Proc. SPIE 4013-56, Munich, Germany, 2000.
11. C. LeBoeuf, P. Davila, et al, "Developmental cryogenic active telescope testbed, a wavefront sensing and control testbed for the next generation space telescope," Proc. SPIE 3356-72, Kona, Hawaii, 1998.
12. P. Davila, A. Lowman, et al, "Optical design of the Developmental Cryogenic Active Telescope Testbed," Proc. SPIE 3356-79, Kona, Hawaii, 1998.
13. E. Young, M. Wilson, et al, "Performance Analysis of the Developmental Cryogenic Active Telescope Testbed (DCATT)," Proc. SPIE 3356-82, Kona, Hawaii, 1998.
14. D. Redding, S. Basinger, et al, "Wavefront Control for the Next Generation Space Telescope," Proc. SPIE 3356-47, Kona, Hawaii, 1998.
15. D. Redding, S. Basinger, et al, "Wavefront Control for a segmented deployable space telescope," Proc. SPIE 4013-115, Munich, Germany, 2000.